Available online at www.sciencedirect.com

ScienceDirect

journal homepage: www.elsevier.com/locate/ijrefrig

# Experimental investigations on thin polymer desiccant wheel performance

Tao Cao [a], Hoseong Lee [a], Yunho Hwang [a,*], Reinhard Radermacher [a], Ho-Hwan Chun [b]

[a] Center for Environmental Energy Engineering, University of Maryland, 4164 Glenn L. Martin Hall Bldg., College Park, MD 20742, USA

[b] Advanced Ship Engineering Research Center (ASERC), Dept. of Naval Architecture & Ocean Engineering, Pusan National University, 30 Changjeon-dong, Kumjeng-ku, Busan 609-735, Republic of Korea

ARTICLE INFO

*Article history:*
Received 18 November 2013
Received in revised form
10 April 2014
Accepted 5 May 2014
Available online 24 May 2014

*Keywords:*
Desiccant wheel
Experimental study
Moisture removal capacity
Latent coefficient of performance

ABSTRACT

In this study, the performance of a new polymer desiccant wheel (DW), which can be used for dehumidification in a solid desiccant cooling system, was investigated. In order to investigate the compact design of the DW for compact cooling system, DWs were evaluated at four levels of thickness while varying the inlet air temperature, humidity ratio, regeneration temperature, and rotational speed. It was found that lower inlet air temperature and higher humidity ratio are in favor of better DW performance. Higher regeneration temperature (60 °C) would bring a reduced marginal benefit in terms of latent coefficient of performance ($COP_{latent}$). Test results also indicate that the optimum rotational speed decreases while DW thickness increases. Three thin DWs (30, 50 and 70 mm) were compared with the typical thick DW (150 mm) and it was found that 50 and 70 mm DWs have the potentials in the compact cooling system with the maximum moisture removal capacity ($MRC_{max}$) based on specific volume ($MRC_{max}$/DW Volume) 1.2 and 0.7 times higher than that of 150 mm DW, respectively. In addition, the maximum $COP_{latent}$ of 50 and 70 mm DW can be up to 0.45 and 0.5, respectively.



# Investigations expérimentales de la performance de roues déshydratantes minces en polymères

*Mots clés* : Roue déshydratante ; Etude expérimentale ; Capacité de déshumidification ; Coefficient de performance latent

* *Corresponding author*. Center for Environmental Energy Engineering (CEEE), Department of Mechanical Engineering, University of Maryland, 4164 Glenn. L. Martin Hall Building, College Park, MD 20742, USA. Tel.: +1 301 405 5247; fax: +1 301 405 2025.
E-mail address: yhhwang@umd.edu (Y. Hwang).

http://dx.doi.org/10.1016/j.ijrefrig.2014.05.004
0140-7007/

**Nomenclature**

*Symbols*

| | |
|---|---|
| $T_{p\_in}$ | process air inlet temperature (°C) |
| $T_{p\_out}$ | process air outlet temperature (°C) |
| $w_{p\_in}$ | process air inlet humidity ratio (gw kga$^{-1}$) |
| $w_{p\_out}$ | process air outlet humidity ratio (gw kga$^{-1}$) |
| $w_{r\_in}$ | regeneration air inlet humidity ratio (gw kga$^{-1}$) |
| $V_{face}$ | face air velocity (m s$^{-1}$) |
| $T_{gen}$ | regeneration temperature (°C) |
| $R_{speed}$ | rotational speed (RPH) |
| $h_{fg}$ | enthalpy of evaporation (water) (kJ kg$^{-1}$) |
| $\dot{m}_p$ | mass flow rate of process air (m$^3$ s$^{-1}$) |
| $\dot{m}_r$ | mass flow rate of regeneration air (m$^3$ s$^{-1}$) |
| $W_{in}$ | power input of the electric heater (kW) |
| $\Delta u$ | uncertainty of u |
| $\Delta x$ | uncertainty of x |
| $\Delta y$ | uncertainty of y |
| $\Delta z$ | uncertainty of z |

*Acronyms*

| | |
|---|---|
| DW | desiccant wheel |
| MRC | moisture removal capacity (g s$^{-1}$) |
| MRR | moisture removal regeneration (g s$^{-1}$) |
| RTD | resistance temperature detectors |
| RH | relative humidity (%) |
| DP | differential pressure (Pa) |
| DAQ | data acquisition system |
| COP | coefficient of performance (dimensionless) |
| $COP_{latent}$ | latent coefficient of performance (dimensionless) |
| SER | sensible energy ratio (dimensionless) |
| RPH | revolution per hour (rev hr$^{-1}$) |
| $MRC_{max}$ | maximum moisture removal capacity (g s$^{-1}$) |
| $COP_{latent\_max}$ | maximum latent coefficient of performance (dimensionless) |

## 1. Introduction

In hot and humid regions, removing moisture from the air accounts for a considerable portion of the air conditioning load. Most air conditioning systems have to lower the air temperature below its dew point to accomplish dehumidification. Solid desiccant cooling has been proposed as an alternative to vapor compression refrigeration for space cooling. It is an environmentally beneficial solution since no ozone depleting refrigerants are needed. Instead, low temperature heat sources, like waste heat from engine or solar heat, can be used to operate the system. Desiccant wheels (DW) are used for dehumidification of the humid air. While silica gel is the most commonly used desiccant material, new materials have been developed and tested. Jia et al. (2006) compared two DW materials which were silica gel and a newly developed composite material (mixture of silica gel and lithium chloride). They reported that the newly developed composite desiccant wheel performed better than the conventional one, and can remove 50 percent more moisture. White et al. (2011) studied two materials (zeolite and a superabsorbent polymer), and compared them with silica gel. They found that these two materials were more effective in dehumidification than silica gel at low regeneration temperature (50 °C) and high relative humidity (higher than 60 percent). Lee and Lee (2012) tested a newly developed desiccant material – a superabsorbent polymer and found that it had two to three times higher sorption capacity. Qian et al. (2013) conducted an experimental investigation on the performance of an adsorption chiller with zeolite, which works well at a low regeneration temperature and is also one of commonly used desiccant materials.

Lots of experimental studies have been conducted to investigate the performance of DWs. Ahmed et al. (2005) conducted the evaluation and optimization of a solar DW performance. A numerical model was developed and validated with experimental data. Moreover, parametric studies were conducted to investigate the effects of the design parameters such as rotational speed, regeneration to adsorption area ratio, and the operating parameters such as air flow rate, inlet air humidity ratio, and regeneration air temperature on the wheel performance. Enteria et al. (2010) evaluated the desiccant wheel based on its moisture removal capacity (MRC) and moisture removal regeneration (MRR). Eicker et al. (2012) investigated several commercially available desiccant wheels, and determined the best rotational speeds for different DWs. Angrisani et al. (2012) conducted an experimental analysis of the DW, which focused on the variations of the performance as a function of the process and regeneration air flow rates. The desiccant material was regenerated by low temperature thermal energy from a micro co-generator. Angrisani et al. (2013) also conducted experimental tests on a silica gel DW to highlight the effect of rotational speed on its performance. Narayanan et al. (2013) designed a non-adiabatic DW and examined its performance through mathematical models and experimental testing. The new design could increase the dehumidification level by around 45 to 53 percent.

Mathematical models of DW have been developed to effectively predict DW performance in a reasonable computation time. There are multiple modeling studies on DW in recent years. Wrobel et al. (2013) validated a simplified model based on the results of the physical model for a DW. Yamaguchi and Saito (2013) established mathematical model to predict silica gel DW performances. Their predicted results were similar to their measured results. The recorded differences were 3.3% for humidity ratio and 10.8% for temperature. De Antonellis and Joppolo (2010) developed a one dimensional model to solve heat and mass transfer within a DW. The model supported a wide range of working conditions and sorption wheel configurations. The performance criteria were also introduced and discussed based on simulation results. Ghiaus et al. (2013) proposed a state space model for a DW control with two approaches – black box and gray box. The gray box has fewer requirements for parameter identification than black box approach. Chunga and Lee (2009) optimized the performance of a DW by using an unsteady one-dimensional numerical model. The optimum condition was determined

**Table 1 – Distinguished features of literature.**

| Author (year) | Regeneration temperature (°C) | Material | Dimensions (diameter/thickness) (mm) |
|---|---|---|---|
| Subramanyam et al. (2004) | Lower than 30 | Metal silicate synthesized on inorganic fiber substrate | 450/200 |
| Ahmed et al. (2005) | 60–90 | Galvanized iron | 700/200 |
| Jia et al. (2006) | 60–120 | Silica gel | 400/200 |
| | | Silica gel & lithium chloride | |
| Enteria et al. (2010) | 60, 70, 80 | Silica-gel | 300/100 |
| White et al. (2011) | 50, 80 | Zeolite and superabsorbent polymer | 300, 360 |
| Enteria et al. (2012) | 60–80 | Silica-gel, Titanium dioxide | – |
| Eicker et al. (2012) | 45–90 | Titanium silicate | 870/140 |
| | | Lithium chloride | 895/250 |
| | | Silica gel | 260/16.6100 |
| | | Silica gel & lithium chloride | 260/16.6100 |
| Angrisani et al. (2012) | 65 | Silica-gel | 700/200 |
| Angrisani et al. (2013) | 60–70 | Silica-gel | 700/200 |
| Wrobel et al. (2013) | 45–50 | Lithium chloride (LiCl) | 650/200 |
| Yamaguchi and Saito (2013) | 50–80 | Glass fiber | 350/20, 60, 100, 200, 400 |

by maximizing MRC under different regeneration temperatures (50–150 °C) and desiccant isotherm shapes. Aprile and Motta (2013) carried out gray-box modeling of a silica gel desiccant wheel for a full-scale desiccant evaporative cooling system. An accurate response model including inlet temperature and rotational speed, was proposed and tested in a wide range of operating conditions. Ruivo et al. (2012) applied the effectiveness method to predict the influence of inlet conditions on the behavior of DW. Several interpolation approaches were evaluated and compared with a numerical model. Chung et al. (2009) optimized the rotational speed and regeneration to process area ratio for a range of regeneration temperatures on the basis of maximum MRC. Ali Ali et al. (2013) presented a model to predict a DW performance under transient conditions. The model was capable of estimating the optimal rotational speed and pressure drop of the DW. The simulation results of the model corresponded to the published data. Wang et al., (2013) proposed a model to control indoor air humidity with a DW. This experiment was conducted to illustrate the applications of the model's predictive control strategy. Goldsworthy and White (2012) developed a numerical model to investigate the influence of the desiccant equilibrium adsorption isotherms on the overall wheel performance. They found the extent of dehumidification was limited primarily by thermal affects caused by both the exothermic adsorption process and the carryover of heat from the regeneration stream. Panaras et al. (2010) investigated a simplified approach for DW modeling. The experimental analysis covered a wide range of operating conditions including flow rate, temperature, and humidity.

The desiccant wheel has been widely used and investigated in various hybrid cooling systems. Models and experimental studies on the system's performance are necessary for improving the system design and commercialization. Subramanyam et al. (2004) discussed integrating a desiccant in an air-conditioner to decrease humidity. The supply air was dehumidified by the desiccant wheel, and the return air from the space was used to regenerate the DW. Enteria et al. (2012) evaluated the solar-desiccant cooling system performance with a new desiccant material (titanium dioxide) at different climates in East-Asia. Finocchiaro et al. (2012) investigated an innovative desiccant cooling cycle using wet heat exchangers. A temperature ranging from 21 to 22 °C could be achieved by the optimization of the indirect cooling process. The electricity consumption was also greatly reduced compared to the previous prototype. Chung and Lee (2011) analyzed the effect of eleven design parameters on the performance of a desiccant cooling system under two different system configurations. They found that the regenerative temperature was the most dominant factor. Sheng et al. (2013) proposed a high temperature heat pump, a DW system, and an air condition unit to meet space cooling and heating demands. The COP of the whole system was 2.08.

Table 1 shows a summary of the recent experimental studies on desiccant wheels, and lists the regeneration temperature, desiccant materials and dimensions. The literature review showed that most experimental studies were conducted with silica gel at high regeneration temperatures. Also, most DWs are thicker than 100 mm, with large diameters. There are currently limited researches conducted with DWs thinner than 100 mm. In order to have compact system packaging, a thin DW is required. Although Eicker et al. (2012) and Yamaguchi and Saito (2013) experimented with thin DWs, they only focused on high regeneration temperature (80 °C). No other study on the potential of thin DWs has been found. In order to respond to this research gap, we investigated the performance of thin polymer DWs with low regeneration temperatures (40, 50, and 60 °C). In this study, the effects of inlet air temperature, humidity ratio, regeneration temperature, and rotational speed on the DW performance were evaluated. Moreover, the performances of thin DWs (30 mm, 50 mm and 70 mm) were compared with that of the typical thickness DW (150 mm thickness), and then the potential of the thin DWs in compact cooling and dehumidification systems was discussed.

## 2. Experimental setup

### 2.1. *Test facility*

Fig. 1 shows the schematic diagram of the experimental setup. A counter flow design was applied between the two air

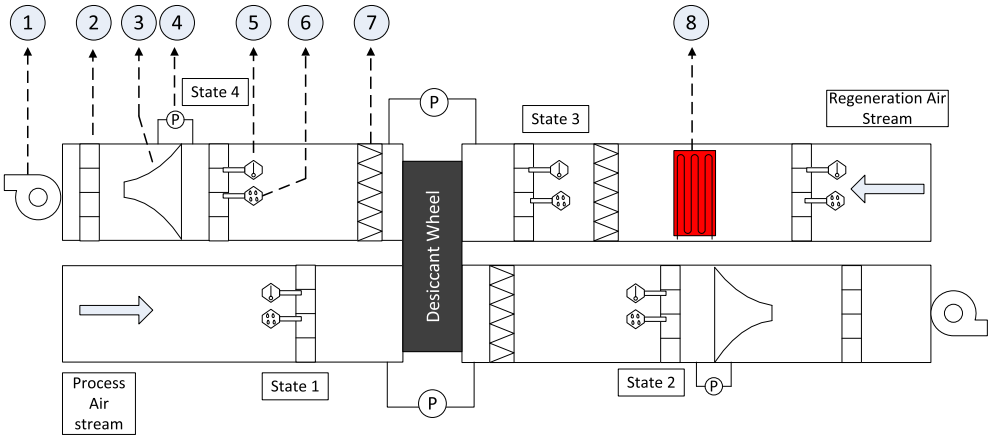


**Fig. 1 – Schematics for polymer desiccant wheel testing system. (① fans; ② straightener; ③ nozzles; ④ differential pressure transducers; ⑤ thermocouple grids; ⑥ humidity sensors; ⑦ air mixers; ⑧ electric heaters.)**

streams across the desiccant wheel. Two wind tunnels were constructed with polypropylene boards to simulate regeneration air and process air streams. Two variable speed fan motors were installed in the downstream of both tunnels to regulate the air flow rates. The desiccant wheel used was a cylindrical shape with honeycomb-shaped cells, which slowly rotates as it continuously dehumidifies the incoming process airstream. The test facility was placed in an environmental chamber where the inlet temperature and relative humidity could be controlled.

For the process air stream, a relatively high humid air enters the DW and moisture is adsorbed by the desiccant. The air then passes through the nozzle to measure the air flow rate and exits the tunnel. The temperatures and humidity's of inlet and outlet of both air streams, and pressure drop across the nozzles and the DW were measured. For the regeneration air stream, an electric heater was used to simulate the regeneration heat source and control the regeneration air stream to the target temperature. The high temperature, low humidity air then enters the DW and moisture is released from the desiccant. The air exiting the DW passes through the nozzle and exits the tunnel, similarly to the process air stream. The testing facility was designed according to ANSI/ASHRAE 41.2-1987 (RA 92) – standard methods for laboratory air flow measurement (ASHRAE, 1992).

An effort was made to minimize the air leakage between the process and regeneration air streams, which can degrade the desiccant DW's performance by increasing process air outlet temperature. Air leakage can also decrease the reliability of test results. The DW case contained two aluminum frame plates, four layers of sealing gaskets (two are silicone foam and the other two are glass fiber), three steel threaded rods, three springs and six nuts. The DW was located in the middle. Two layers of glass fiber gaskets were attached to both surfaces of the DW. They can provide a smooth surface, allowing the DW to rotate with a minimum friction. The silicone foam gaskets were used next to the glass fiber gaskets. The aluminum frame plates were then attached to the silicone foam gaskets. Three steel threaded rods were used to hold the DW and gaskets. Two nuts were used in both ends of each bolt rod to lock them into place. The springs were used to apply pressure force on the plates against the DW.

### 2.2. *Measurement*

T-type thermocouples were used for temperature measurement in all state points. In addition, resistance temperature detectors (RTD) and relative humidity (RH) sensors were also used to measure air stream temperatures and RHs. For the thermocouples, a nine-point grid system was used, which contained nine evenly distributed thermocouples. The average values of the nine thermocouples were taken as a final temperature reading. The readings of thermocouple grids and RTDs were compared, and the temperature differences were within 0.2 °C. The RH sensors were installed in the center of air flow stream, next to thermocouple grids. All properties obtained such as temperatures and RHs were used to evaluate the psychometric properties including humidity ratio and enthalpy. Differential pressure (DP) transducers were employed to obtain the mass flow rates of two air streams, and to quantify the pressure drop across the DW. The power consumption of the electric heater was measured with digital

**Table 2 – Specifications of sensors.**

| Sensors | Manufacturer | Model no. | Measurement range | Systematic error |
|---|---|---|---|---|
| Thermocouple | Omega | T type | −185–300 °C | ±0.5 °C |
| DP transducer | Setra | 264 | 623 Pa | ±1.0% FS |
| RH sensor | Vaisala | HMT313 | 0–100% RH | ± (1.0 + 0.008 × reading) % RH |
| RTD | Vaisala | HMT313 | −20–80 °C | ±0.25 °C |
| Watt meter | Ohio Semitronics | GH-019D | 0–4 kW | ± (0.2% reading + 0.05% FS) |

**Table 3 – Specifications of desiccant wheels.**

| No. | Material | Diameter (mm) | Thickness (mm) |
|---|---|---|---|
| 1 | Polymer | 300 | 30 |
| 2 | Polymer | 300 | 50 |
| 3 | Polymer | 300 | 70 |
| 4 | Polymer | 350 | 150 |

watt meters. With known temperatures before and after the heater, the mass flow rate of regeneration air upstream could be obtained. Specifications of sensors are provided in Table 2. The RH, DP sensors, and air flow rate were calibrated under testing conditions.

### 2.3. Test procedure and conditions

The data acquisition system (DAQ) was established with LabVIEW 2013, which can control the relative humidity, temperature, and mass flow rate of all four state points. Table 3 shows the specifications of the four DWs tested. All of the DWs were made of polymer material and had the same diameter, except for the 150 mm thick DW. The thicknesses varied from 30 to 150 mm. The first three were considered as thin DWs as they were thinner than 100 mm. The test matrix is provided in Table 4. For each condition, seven different rotational speeds were used. Initially, the chamber was turned on and set to the desired temperature and humidity conditions. After that, both fan motors and DW motor were turned on. Once the desired air conditions were reached, the electric heater was turned on to obtain the desired regeneration temperature. After steady state conditions had been achieved, data were recorded for 30 min with a one-second time interval.

## 3. Methodology

### 3.1. DW performance evaluation indices

The moisture removal capacity quantifies the amount of moisture removed from the processing stream as it passes through the DW, given by Eq. (1).

$$\mathrm{MRC} = \dot{m}_{\mathrm{p}}\left(\omega_{\mathrm{p\_in}} - \omega_{\mathrm{p\_out}}\right) \tag{1}$$

The latent coefficient of performance ($\mathrm{COP_{latent}}$) relates the changes in latent energy along the processing stream to the energy input required to regenerate the desiccant, given by Eq. (2). The $W_{in}$ is the power consumption of electric heater.

$$\mathrm{COP_{latent}} = \frac{\dot{m}_{\mathrm{p}} h_{\mathrm{fg}}\left(\omega_{\mathrm{p\_in}} - \omega_{\mathrm{p\_out}}\right)}{W_{\mathrm{in}}} \tag{2}$$

The MRC and $\mathrm{COP_{latent}}$ are the most commonly used indicators when evaluating the performances of a DW. The values of MRC and $\mathrm{COP_{latent}}$ increase as the dehumidification capacity increases at a given heat input, making it a more efficient system. However, the MRC and $\mathrm{COP_{latent}}$ usually reach their maximum under different testing conditions, which is discussed in the experiment results section.

The sensible energy ratio (SER) is also used when evaluating the DWs. During the dehumidification of processed air, energy is released from the desiccant wheel as a result of the adsorption process, as well as the unintentional heat transfer from the regeneration air stream to the process air stream due to the temperature differences between the two. Therefore, the SER can quantify this additional sensible load to be handled by some additional cooling mechanism at the downstream such as an evaporative cooling or a vapor compression cycle. Lower values of SER mean that the DW is creating a lower sensible cooling load, which indicates better performance of the DW. The SER is given by Eq. (3).

$$\mathrm{SER} = \frac{\dot{m}_{\mathrm{p}}\left(T_{\mathrm{p\_in}} - T_{\mathrm{p\_out}}\right)}{\dot{m}_{\mathrm{r}}\left(T_{\mathrm{p\_in}} - T_{\mathrm{gen}}\right)} \tag{3}$$

In this study, the performance of four DWs was evaluated with varying thicknesses: 30, 50, 70, and 150 mm. The DW with 150 mm thickness had a larger diameter (350 mm) than the other three DWs (300 mm). Since the air flow rate was maintained at constant throughout all tests, the face velocity of 150 mm DW was lower (2.0 m $s^{-1}$) than the other three DWs (2.8 m $s^{-1}$). To ensure thickness was the only variable, we converted the MRC test data of the 350 mm diameter DW to that of the 300 mm diameter DW, while maintaining the same face velocity with the other three DWs. An example of MRC conversion equation is given in Eq. (4).

$$\mathrm{MRC_{new}} = \mathrm{MRC_{old}}\frac{300^2}{350^2} \times \frac{2.8}{2} \tag{4}$$

### 3.2. Uncertainty analysis

The experimental error can be classified into two broad categories: systematic error and random error, which typically accounts for the uncertainty of the acquired data (Linberg 2000). The systematic error is associated with the various instrumentation precisions, manifested in temperature, pressure, and relative humidity measurements. The random error pertains to the acquired data deviation from the mean value. Performance indices, or dependent variables, are correlated with the error propagation of the individual measurement uncertainties. The general error propagation is given by Eq. (5). Here u is a function of x, y and z. Δu is the uncertainty of u, similar to Δx, Δy and Δz.

$$\Delta u = \sqrt{\left(\frac{\partial u}{\partial x}\right)^2 \cdot (\Delta x)^2 + \left(\frac{\partial u}{\partial y}\right)^2 \cdot (\Delta y)^2 + \left(\frac{\partial u}{\partial z}\right)^2 \cdot (\Delta z)^2} \tag{5}$$

An example for the propagated error, pertaining to MRC is given below by Eq. (6).

$$\Delta\mathrm{MRC} = \sqrt{\left(\omega_{\mathrm{p\_in}} - \omega_{\mathrm{p\_out}}\right)^2 \cdot \left(\Delta\dot{m}_{\mathrm{p}}\right)^2 + \left(\dot{m}_{\mathrm{p}} \cdot \omega_{\mathrm{p\_out}}\right)^2 \cdot \left(\Delta\omega_{\mathrm{p\_in}}\right)^2 + \left(\dot{m}_{\mathrm{p}} \cdot \omega_{\mathrm{p\_in}}\right)^2 \cdot \left(\Delta\omega_{\mathrm{p\_out}}\right)^2} \tag{6}$$

**Table 4 – Test matrix.**

| No. | $T_{p\_in}$ | $w_{p\_in}$ | $w_{r\_in}$ | Volume flow rate | | $T_{gen}$ | $R_{speed}$ | Test duration |
|---|---|---|---|---|---|---|---|---|
| | °C | gw kga$^{-1}$ | gw kga$^{-1}$ | m$^3$·s | m$^3$ hr$^{-1}$ | °C | RPH | min |
| 1 | 25 | 15 | 15 | 0.10 | 360 | 60 | 10 to 70 with 10 steps | 30 |
| 2 | 30 | 15 | 15 | 0.10 | 360 | 60 | | 30 |
| 3 | 35 | 15 | 15 | 0.10 | 360 | 60 | | 30 |
| 4 | 30 | 10 | 10 | 0.10 | 360 | 60 | | 30 |
| 5 | 30 | 20 | 20 | 0.10 | 360 | 60 | | 30 |
| 6 | 30 | 15 | 15 | 0.10 | 360 | 50 | | 30 |
| 7 | 30 | 15 | 15 | 0.10 | 360 | 40 | | 30 |

## 4. Experimental Results

Although all the DWs were tested with varying process air inlet temperatures, inlet humidity ratios, and regeneration temperatures, only the results of the 50 mm thickness DW were discussed in detail since the DWs showed similar trends with these three factors. In the last section, we examined the effects of DW thicknesses (30, 50, 70 and 150 mm).

### 4.1. *Effect of process air inlet temperature*

The effects of the process air inlet temperature was investigated (test 1, 2, 3 in Table 4) and shown in Fig. 2. The process air inlet temperature was varied, while the inlet humidity ratio and regeneration temperature remained constant. The relative humidity of regeneration air after heater also remained constant (12 percent). As the process air inlet temperature increased, the MRC decreased as shown in Fig. 2(a). At a rotational speed of 50 RPH, the MRC decreased from

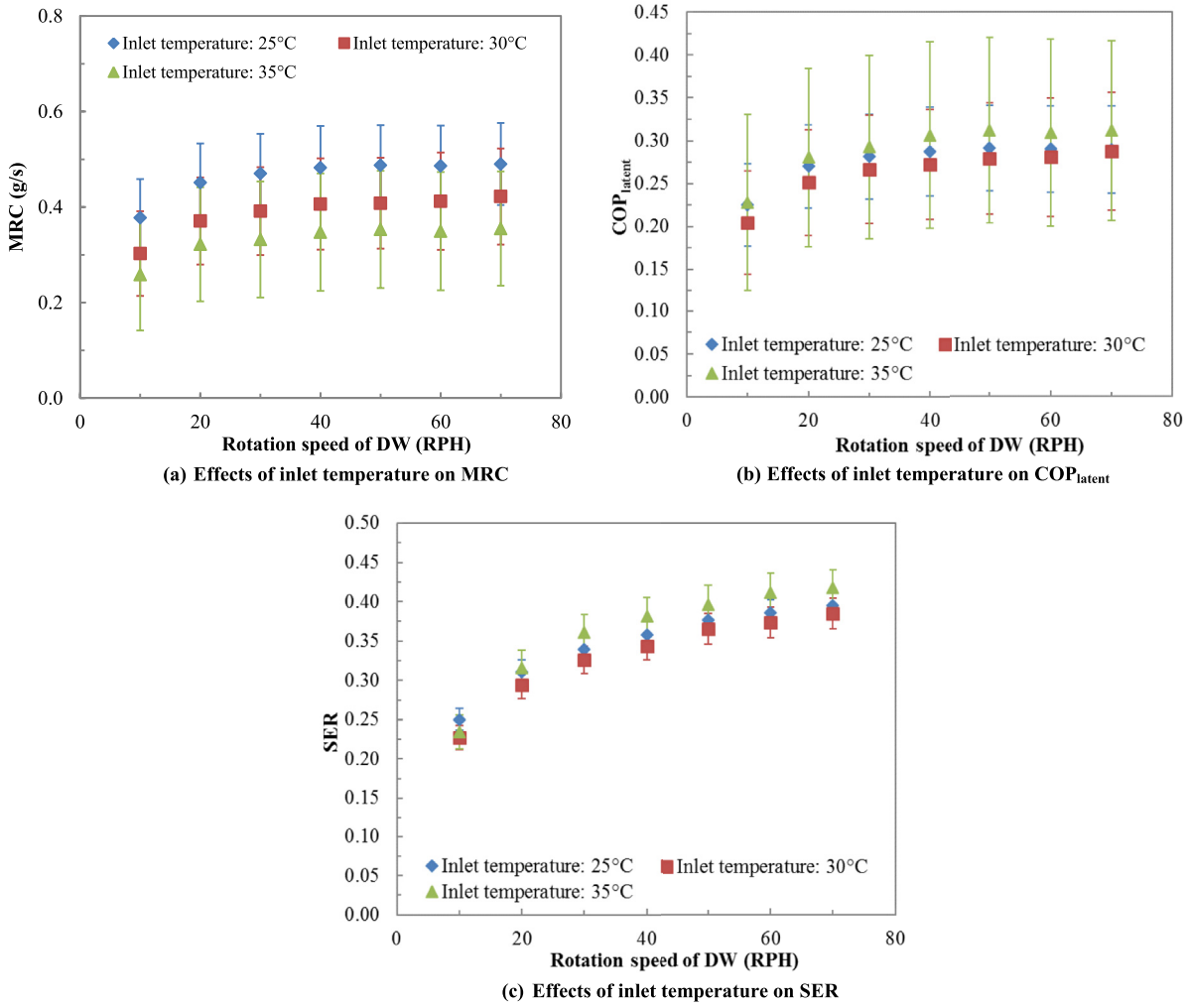


**Fig. 2 – Effects of inlet temperature on 50 mm DW performance (a) Effects of inlet temperature on MRC (b) Effects of inlet temperature on $COP_{latent}$ (c) Effects of inlet temperature on SER.**

0.488 g $s^{-1}$ to 0.353 g $s^{-1}$, while inlet temperature increased from 25 °C to 35 °C. When the humidity ratio is fixed, the vapor pressure in the process air remains constant. Higher dry bulb temperature increases the saturated vapor pressure of the desiccant. The saturated vapor pressure is the driving force for moisture transfer. Higher values of saturated vapor pressure indicate lower tendency for water vapor to condense and be adsorbed by desiccant material. Therefore, warmer air results in a reduced adsorption rate, removes less air and leads to lower MRC when the humidity ratio is fixed. Generally, there is an optimum RPH of the DW maximizing the MRC. If the rotational speed is too low, the desiccant wheel may not perform to its maximum capacity as adsorption and desorption processes already saturated before the process and regeneration areas switch. Alternatively, if the rotational speed is too high, the desiccant material cannot fully adsorb or desorb water vapor due to the short process time. As shown in Fig. 2(b), the $COP_{latent}$ reacts similarly to MRC as rotational speed increases, but is less sensitive to inlet temperature.

As for the SER, it increases with rotational speed. This is due to the increased sensible heat transfer between the regeneration and process air streams. When the temperature difference between the regeneration and process air streams is fixed, the sensible heat flux, which is defined as the sensible heat transfer rate per unit area, is fixed. The sensible heat transfer rate is the heat transferred per unit time, and is proportional to the product of the sensible heat flux and rotational speed. Higher rotational speed increases the sensible heat transfer rate as it increases the heat transfer areas per unit time. In other words, the high rotational speed increases the process air outlet temperature. There is no significant variation in SER with process air inlet temperatures.

The error bars are also shown for all data points. It is found that the MRC and COP have high relative uncertainties, ranging from 25 to 40 percent. The major contribution (80–90 percent) comes from the measurement error of relative humidity. SER only involves temperature measurement, so the relative errors are roughly 10 percent.

### 4.2. *Effect of the process air humidity*

The effect of the process air inlet humidity was investigated (test 2, 4, 5 in Table 4) as shown in Fig. 3. The process air inlet humidity ratio varied while the inlet and regeneration

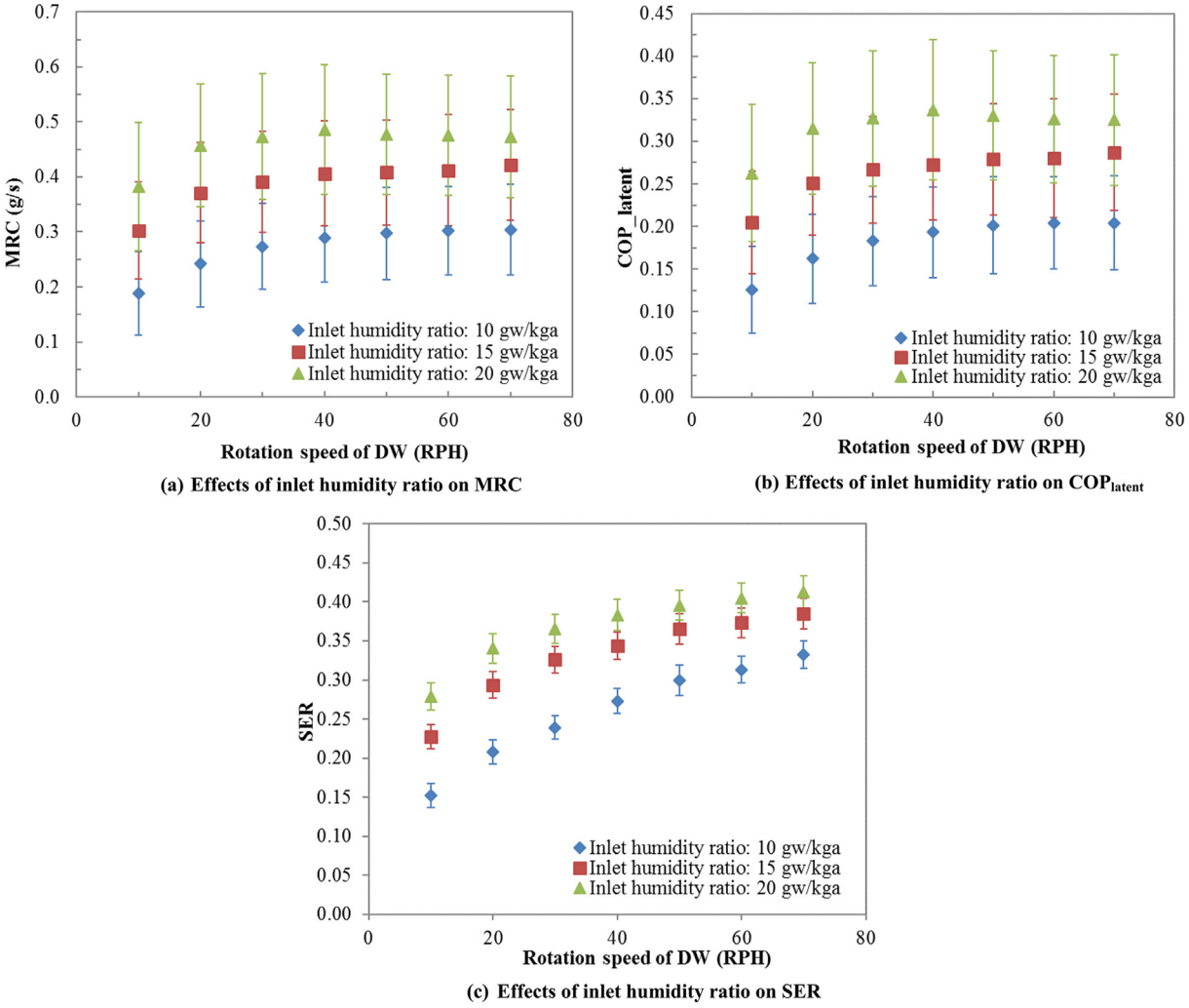


**Fig. 3 – Effects of inlet humidity ratio on 50 mm DW performance (a) Effects of inlet humidity ratio on MRC (b) Effects of inlet humidity ratio on $COP_{latent}$ (c) Effects of inlet humidity ratio on SER.**

temperatures were fixed at 30 °C and 60 °C, respectively. The relative humidity of regeneration air after it has been heated increased from 8 percent to 15 percent with increasing inlet humidity ratios. As the humidity ratio increased, the MRC increased as shown in Fig. 3(a). Increased humidity ratio indicates higher partial pressure of water vapor, which means higher tendency for water to condense and be adsorbed by the desiccant material, thus larger driving force for adsorption. MRC displayed similar trends with increasing rotation speeds, as discussed in chapter 4.1. Similar to MRC, a higher latent performance was achieved at higher inlet humidity ratio. For instance, the MRC and $COP_{latent}$ increased by 68 and 74 percent, respectively, at a rotational speed of 40 RPH when the humidity ratio increased from 10 gw $kga^{-1}$ to 20 gw $kga^{-1}$. The SER slightly increased with rotational speed.

### 4.3. *Effect of regeneration temperature*

The effect of the regeneration air inlet temperature was investigated (test 2, 6, 7 in Table 4) as shown in Fig. 4. The regeneration air inlet temperature varied while the temperature and humidity ratio of inlet air remained constant. As the regeneration temperature increased, the MRC increased. Also, MRC increase slows down at higher regeneration temperature. As an example, at 10 RPH, MRC increase from 50 °C to 60 °C is only about 60 percent of that from 40 °C to 50 °C. For the $COP_{latent}$, as the regeneration temperature decreased, the desiccant latent performance increased because the MRC increased at a rate lower than that of the regeneration temperature.

The sensible effectiveness decreased with regeneration temperature. Although higher regeneration temperature results in higher process outlet air temperature, the SER decreased due to larger difference between regeneration and process inlet temperatures. The SER reached its saturated state at a low regeneration temperature and a high rotational speed, as shown in Fig. 4(c), since heat transfer through adsorption and desorption processes reached their maximum rates.

As discussed before, higher regeneration temperature resulted in higher MRC but lower $COP_{latent}$. A high regeneration temperature resulted in a reduced marginal benefit, with respect to the latent performance. In our testing, a 50 °C regeneration temperature was the optimum working

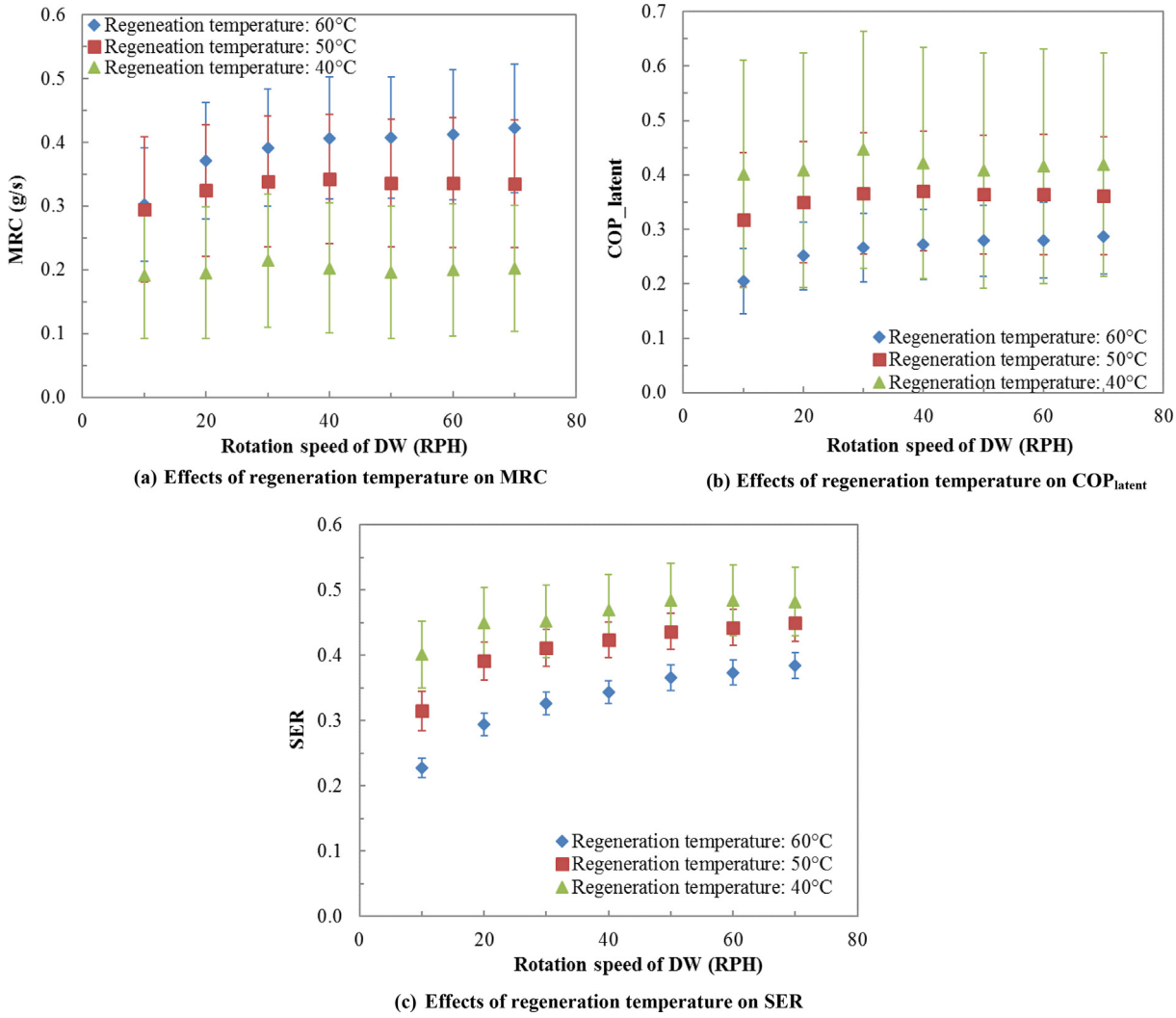


(a) Effects of regeneration temperature on MRC

(b) Effects of regeneration temperature on $COP_{latent}$

(c) Effects of regeneration temperature on SER

**Fig. 4 – Effects of regeneration temperature on 50 mm DW performance (a) Effects of regeneration temperature on MRC (b) Effects of regeneration temperature on $COP_{latent}$ (c) Effects of regeneration temperature on SER.**

condition because it can provide good MRC and $COP_{latent}$ simultaneously. A 50 °C heat source can be obtained through a solar thermal collector or through waste heat from an engine and viewed as low degrade heat.

### 4.4. *Effect of DW thickness on the performance*

In this section, we focused on the effects of different DW thicknesses and selected test 5 conditions in Table 4 (process air inlet temperature 30 °C, inlet humidity ratio 20 gw $kga^{-1}$, regeneration temperature 60 °C) for all DWs. As the DW thickness increased, the MRC can be expected to increase. In order to reach full potential in capacity, the DW has to rotate slowly enough to provide a sufficient amount of time for adsorption and desorption processes, which are essential for moisture transfer from the process air to the regeneration air. This explains why DWs peak earlier in MRC with increasing thicknesses, as shown in Fig. 5(a). For instance, 150 mm MRC peaks at 10 RPH, while 30 mm peaks at 70 RPH. The $COP_{latent}$ displays similar trends with rotational speed for each desiccant wheel and with increased thicknesses, as shown in Fig. 5(b). Increased thickness means the DW can hold more heat from the regeneration air, thus allows more heat transfer between the process and the regeneration air streams. Therefore, the SER increases with thicknesses.

Table 5 shows the maximum MRC, $COP_{latent}$, minimum SER and pressure drop across DW for all four DWs. The corresponding conditions are also listed in the order of rotational speed, process air inlet temperature, humidity ratio, and regeneration temperature. As discussed before, the maximum MRC and $COP_{latent}$ increased with thicknesses. The SER also increased rapidly with thickness. While this is not the major concern for the DW operation, it could be one of the main issues in integrated cooling and dehumidification system design. When the process inlet and regeneration temperature are fixed, higher SER leads to higher process outlet temperature. Thus higher sensible cooling load is added by the DW in the dehumidification process. The DW is typically used in the hybrid cooling system to handle the latent cooling load. As a result, the device located in the downstream of DW, which is usually a vapor compression chiller, can be used to handle only sensible cooling load. The extra sensible cooling load created by the DW is not desired and increased the amount of the workloads for vapor compression chiller. Thus the whole

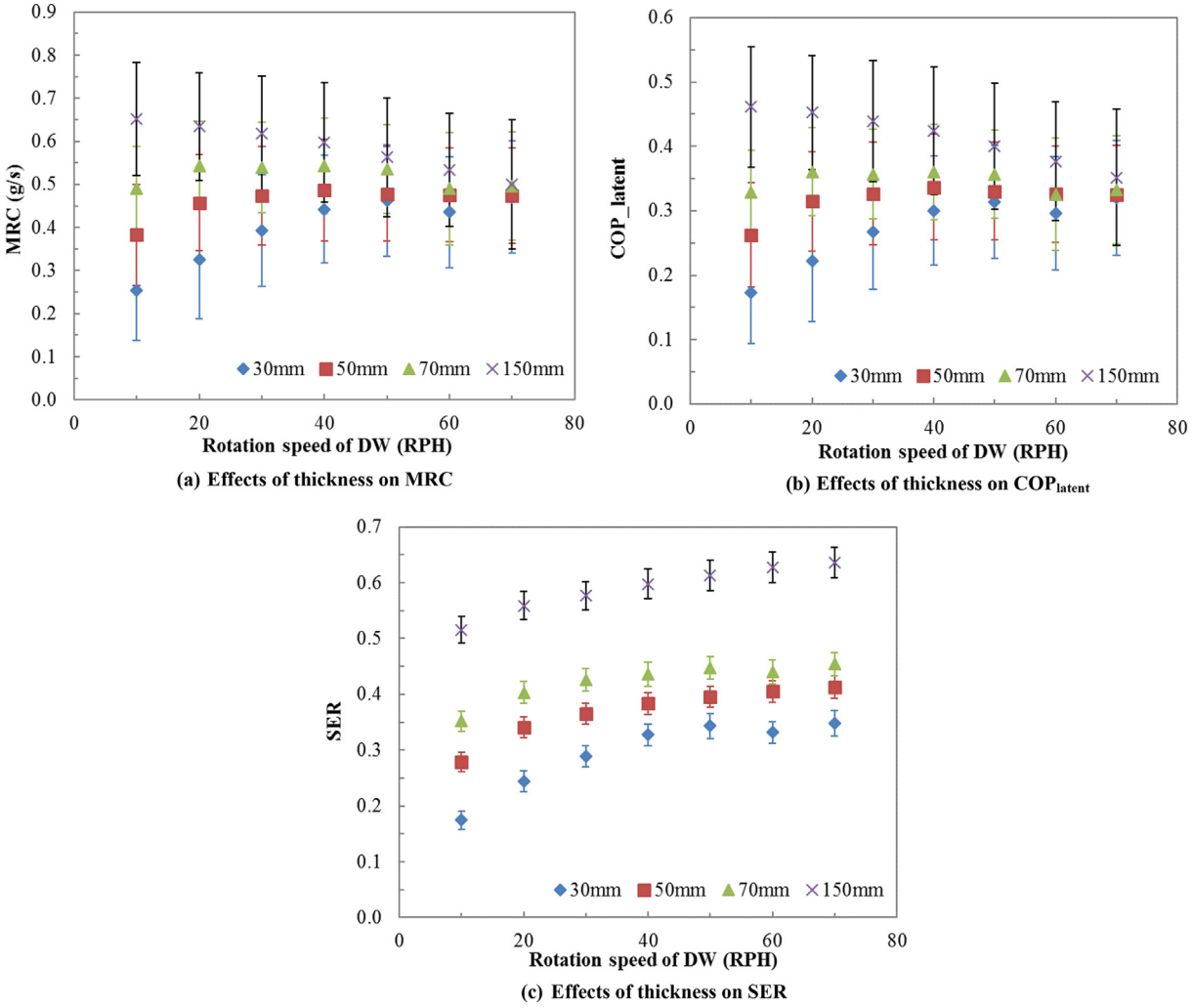


**Fig. 5 – Effects of thickness on DW performance. (a) Effects of thickness on MRC (b) Effects of thickness on $CO_{Platent}$ (c) Effects of thickness on SER.**

**Table 5 – Maximum MRC and COP for all DWs.**

| Indices | 30 mm DW | 50 mm DW | 70 mm DW | 150 mm DW |
|---|---|---|---|---|
| $MRC_{max}$ ($g\ s^{-1}$) | 0.474 (at 70RPH, 25 °C, 15 gw $kga^{-1}$, 60 °C) | 0.490 (at 70RPH, 25 °C, 15 gw $kga^{-1}$, 60 °C) | 0.544 (at 20RPH, 30 °C, 20 gw $kga^{-1}$, 60 °C) | 0.664 (at 20RPH, 25 °C, 15 gw $kga^{-1}$, 60 °C) |
| $MRC_{max}$/Volume ($g\ s^{-1}\ m^{-3}$) | 224 | 139 | 110 | 63 |
| $COP_{latent\_max}$ | 0.381 (at 70RPH, 30 °C, 15 gw $kga^{-1}$, 40 °C) | 0.446 (at 30RPH, 30 °C, 15 gw $kga^{-1}$, 40 °C) | 0.482 (at 30RPH, 30 °C, 15 gw $kga^{-1}$, 40 °C) | 0.591 (at 10RPH, 30 °C, 15 gw $kga^{-1}$, 40 °C) |
| $SER_{min}$ | 0.079 (at 10RPH, 30 °C, 10 gw $kga^{-1}$, 60 °C) | 0.153 (at 10RPH, 30 °C, 10 gw $kga^{-1}$, 60 °C) | 0.211 (at 10RPH, 30 °C, 10 gw $kga^{-1}$, 60 °C) | 0.388 (at 10RPH, 30 °C, 10 gw $kga^{-1}$, 60 °C) |
| Pressure drop across DW (Pa) | 59 | 70 | 100 | 140 |

system requires more power input. Moreover, increased thickness means a significant pressure drop across the DW, thus an increased demand for the fans. The air-side pressure of 150 mm DW was twice of 50 mm DW.

Overall, the thin DWs have the potential to be used in compact dehumidification and cooling systems while satisfying $COP_{latent}$ and lower SER and pressure drop. For example, maximum $COP_{latent}$ for 50 and 70 mm DWs are 0.446 and 0.482, respectively while the expected $COP_{latent}$ of DW system is 0.5. Furthermore, 50 and 70 mm DWs can reduce the pressure drop by 50 and 30 percent, respectively. When viewed on the specific volume basis, the thin DWs outperform the thick DW. For instance, the maximum MRC based on the specific volume of the 50 mm DW is 1.2 times higher than that of 150 mm DW. The reason is that the relative humidity decreases along the DW, thus the dehumidification capacity of the desiccant becomes lower. In other words, for a thick DW, the downstream part of the thick DW does not perform well as the upstream part.

For each DW, the MRC and COP usually reach their respective maximum points at different working conditions as indicated in Table 5. For instance, the 50 mm DW has maximum MRC at 25 °C process inlet temperature, 15 gw $kga^{-1}$ inlet humidity ratio and 60 °C regeneration temperature, while the maximum COP is obtained at 30 °C process inlet temperature, 15 gw $kga^{-1}$ inlet humidity ratio and 40 °C regeneration temperature. This means that when designing a desiccant wheel system, one should be cautious about the optimum working conditions, and a balance between the MRC and COP should be considered.

## 5. Conclusions

The performance of the new polymer desiccant material was investigated experimentally. This desiccant material can be regenerated using a low temperature heat source like 50 °C. The effects of the process air stream's temperature and humidity, the regeneration temperature, the desiccant wheel's rotational speed and the DW thickness were investigated.

Test results show that the MRC is decreased with higher inlet air temperature. This is because of the increased saturated vapor pressure of the desiccant. There was no significant variation in $COP_{latent}$ and SER in regards to process air inlet temperature. Higher humidity ratio resulted in improved MRC and $COP_{latent}$, yet an undesirable SER outcome.

When the regeneration temperature increased, the MRC increased as well. However, the $COP_{latent}$ decreased since the increased rate of MRC was lower than that of regeneration temperature. The SER was lower at higher regeneration temperatures because of the significant differences between the regeneration and the process inlet temperatures. Also, the SER reached saturated points at low regeneration temperature and high rotational speed. A higher regeneration temperature would bring a reduced marginal benefit, with respect to the latent performance.

Generally, there is an optimum rotational speed for the DW performance regarding the MRC and $COP_{latent}$. By comparing four DWs with different thicknesses, it was found that DWs peak in MRC and $COP_{latent}$ at lower rotational speeds with increased thicknesses. Moreover, a DW usually reaches maximum MRC and $COP_{latent}$ at different operating conditions. Therefore, the balance between the MRC and $COP_{latent}$ should be considered when selecting optimum working conditions for the DW. The SER increased with increasing rotational speed and thickness.

Finally, the potentials of thin DWs were demonstrated in compact cooling and dehumidification systems, especially when the dehumidification load could be met with thin DWs without requiring thicker ones. With $COP_{latent}$ (50 and 70 mm) very close to that of the standard thickness DWs, the thin DWs also generate less sensible cooling load and power demand for the fan motors. Moreover, the maximum MRCs of 50 and 70 mm DWs based on specific volume are 120 and 70 percent respectively higher than that of the 150 mm DW. Therefore, a better system performance can be expected.

## Acknowledgments

This work was supported by sponsors of the CEEE, University of Maryland, College Park, MD, USA and partially supported by the National Research Foundation of Korea (NRF) grant funded by the Korea government (MEST) through GCRC-SOP (Grant No. 2012-0004782).

## REFERENCES

Ahmed, M.H., Kattab, N.M., Fouad, M., 2005. Evaluation and optimization of solar desiccant wheel performance. Renew. Energy 30, 305–325.

Ali, Muzaffar, Vukovic, Vladimir, Sahir, Mukhtar Hussain, Basciotti, Daniele, 2013. Development and validation of a desiccant wheel model calibrated under transient operating conditions. Appl. Therm. Eng. 61, 469–480.

Angrisani, G., Minichiello, F., Roselli, C., Sasso, M., 2012. Experimental analysis on the dehumidification and thermal performance of a desiccant wheel. Appl. Energy 92, 563–572.

Angrisani, G., Roselli, C., Sasso, M., 2013. Effect of rotational speed on the performances of a desiccant wheel. Appl. Energy 104, 268–275.

Aprile, Marcello, Motta, Mario, 2013. Grey-box modelling and in situ experimental identification of desiccant rotors. Appl. Therm. Eng. 51, 55–64.

ASHRAE, 1992. Standard 41.2-1987 (RA 92) – Standard Methods for Laboratory Airflow Measurement.

Chung, Jae Dong, Lee, Dae-Young, 2011. Contributions of system components and operating conditions to the performance of desiccant cooling systems. Int. J. Refrigeration 34, 922–927.

Chung, Jae Dong, Lee, Dae-Young, Yoon, Seok Mann, 2009. Optimization of desiccant wheel speed and area ratio of regeneration to dehumidification as a function of regeneration temperature. Sol. Energy 83, 625–635.

Chunga, Jae Dong, Lee, Dae-Young, 2009. Effect of desiccant isotherm on the performance of desiccant wheel. Int. J. Refrigeration 32, 720–726.

De Antonellis, Stefano, Joppolo, Cesare Maria, 2010. Luca Molinaroli, Simulation, performance analysis and optimization of desiccant wheels. Energy Build. 42, 1386–1393.

Eicker, U., Schürger, U., Köhler, M., Ge, T., Dai, Y., Li, H., Wang, R., 2012. Experimental investigations on desiccant wheels. Appl. Therm. Eng. 42, 71–80.

Enteria, N., Yoshino, H., Satake, A., Mochida, A., Takaki, R., Yoshie, R., Mitamura, T., Baba, S., 2010. Experimental heat and mass transfer of the separated and coupled rotating desiccant wheel and heat wheel. Exp. Therm. Fluid Sci. 34, 603–615.

Enteria, N., Yoshino, H., Satake, A., Mochida, A., Satake, A., Yoshie, R., Takaki, R., Yonekura, H., Mitamura, T., Tanaka, Y., 2012. Performance of solar-desiccant cooling system with Silica-Gel (SiO2) and Titanium Dioxide (TiO2) desiccant wheel applied in East Asian Climates. Sol. Energy 86, 1261–1276.

Finocchiaro, Pietro, Beccali, Marco, Nocke, Bettina, 2012. Advanced solar assisted desiccant and evaporative cooling system equipped with wet heat exchangers. Sol. Energy 86, 608–618.

Ghiaus, Christian, Ghazal, Roula, Joubert, Patrice, Hayyani, Mohamed Yasser, 2013. Gray-box state-space model and parameter identification of desiccant wheels. Appl. Therm. Eng. 51, 742–752.

Goldsworthy, M., White, S.D., 2012. Limiting performance mechanisms in desiccant wheel dehumidification. Appl. Therm. Eng. 44, 21–28.

Jia, C.X., Dai, Y.J., Wu, J.Y., Wang, R.Z., 2006. Experimental comparison of two honeycombed desiccant wheels fabricated with silica gel and composite desiccant material. Energy Convers. Manag. 47, 2523–2534.

LabVIEW, 2013. Help, June 2013. Available on the web. http://zone.ni.com/reference/en-XX/help/371361K-01.

Lee, Joohyun, Lee, Dae-Young, 2012. Sorption characteristics of a novel polymeric desiccant. Int. J. Refrigeration 35, 1940–1949.

Linberg, V. Uncertainties and Error Propagation Part 1 of a manual on Uncertainties, Graphing, and the Vernier Caliper, 1 July 2000. Available on the web http://www.rit.edu/cos/uphysics/uncertainties/Uncertaintiespart2.html#addsub.

Narayanan, R., Saman, W.Y., White, S.D., 2013. A non-adiabatic desiccant wheel: modeling and experimental validation. Appl. Therm. Eng. 61, 178–185.

Panaras, G., Mathioulakis, E., Belessiotis, V., Kyriakis, N., 2010. Experimental validation of a simplified approach for a desiccant wheel model. Energy Build. 42, 1719–1725.

Qian, Suxin, Gluesenkamp, Kyle, Hwang, Yunho, Radermacher, Reinhard, Chun, Ho-Hwan, 2013. Cyclic steady state performance of adsorption chiller with low regeneration temperature zeolite. Energy 60, 517–526.

Ruivo, C.R., Carrillo-Andrés, A., Costa, J.J., Domínguez-Mũñoz, F., 2012. Interpolation procedures for the effectiveness method to account for the influence of the inlet airflow states on the desiccant wheels performance. Energy Build. 55, 380–388.

Sheng, Ying, Zhang, Yufeng, Deng, Na, Fang, Lei, Nie, Jinzhe, Ma, Lijun, 2013. Experimental analysis on performance of high temperature heatpump and desiccant wheel system. Energy Build. 66, 505–513.

Subramanyam, N., Maiya, M.P., Murthy, S.S., 2004. Application of desiccant wheel to control humidity in air conditioning systems. Appl. Therm. Eng. 24, 2777–2788.

Wang, Nan, Zhang, Jiangfeng, Xia, Xiaohua, 2013. Desiccant wheel thermal performance modeling for indoor humidity optimal control. Appl. Energy 112, 999–1005.

White, Stephen D., Goldsworthy, Mark, Reece, Roger, Spillmann, Thorsten, Gorur, Abdullah, Lee, Dae-Young, 2011. Characterization of desiccant wheels with alternative materials at low regeneration temperatures. Int. J. Refrigeration 34, 1786–1791.

Wrobel, J., Morgenstern, P., Schmitz, G., 2013. Modeling and experimental validation of the desiccant wheel in a hybrid desiccant air conditioning system. Appl. Therm. Eng. 51, 1082–1091.

Yamaguchi, Seiichi, Saito, Kiyoshi, 2013. Numerical and experimental performance analysis of rotary desiccant wheels. Int. J. Heat. Mass Transf. 60, 51–60.